Nanoscale

PAPER

View Article Online
View Journal | View Issue



Cite this: *Nanoscale*, 2014, **6**, 1525

# From isotope labeled $CH_3CN$ to $N_2$ inside single-walled carbon nanotubes

Christian Kramberger,*[a] Theerapol Thurakitseree,†[b] Erik Einarsson,‡[b] Akito Takashima,[c] Toyohiko Kinoshita,[c] Takayuki Muro[c] and Shigeo Maruyama[b]

Received 4th September 2013
Accepted 22nd October 2013

DOI: 10.1039/c3nr04729f

www.rsc.org/nanoscale

The observation of one-dimensional $N_2$ inside single-walled carbon nanotubes raises the questions, how are the $N_2$ molecules formed and how do they manage to make their way to this peculiar place? We have used $N^{15}$ and $C^{13}$ isotope labeled acetonitrile during the synthesis of single-walled carbon nanotubes to investigate this process. The isotope shifts of phonons and vibrons are observed by Raman spectroscopy and X-ray absorption. We identify the catalytic decomposition of acetonitrile as the initial step in the reaction pathway to single-walled carbon nanotubes containing encapsulated $N_2$.

## 1 Introduction

The ability of multi-walled carbon nanotubes (MWNTs) to encapsulate $N_2$ was first demonstrated in ref. 1. If $N_2$ is enclosed in the as-synthesized MWNTs, the nanotubes exhibit a compartmentalized bamboo structure that traps pockets of $N_2$.[2,3] The detailed distribution of encapsulated $N_2$ and N incorporated into the walls of MWNTs has been directly imaged by polarized scanning transmission X-ray microscopy.[4] The alignment of $N_2$ in the confining walls has also been observed by X-ray absorption.[5,6] A commonly observed effect of using N-containing precursors in the growth of single-walled (SW) and MWNTs by chemical vapor deposition (CVD) is the increased curvature in the emerging $sp^2$ networks. In MWNTs this is seen as a topological curvature resulting in the formation of separate compartments. In SWNTs, however, reducing diameters increase the geometrical curvature.[7–11]

In the case of MWNTs, the $N_2$ gas is partially aligned on the walls of the nano-compartments. For a truly one-dimensional phase of nitrogen, much more narrow single-walled carbon nanotubes with diameters smaller than one nanometer are required. Such configurations of aligned $N_2$ chains have been predicted and expounded using density functional theory.[12] Only recently have one-dimensional, highly aligned $N_2$ inside SWNTs been confirmed by polarized X-ray absorption spectroscopy.[13] The commonly accepted mechanism for the encapsulation of $N_2$ has been put forth in ref. 14. Very briefly, C≡N radicals react inside the catalyst particle and release $N_2$, which then emerges into the currently growing compartment. While the correlation of encapsulated $N_2$ with the use of N containing precursors is generally accepted, direct identification of the reaction pathway by isotope labeling has not yet been achieved. Moreover, it remains an open issue whether or not the proposed C≡N radicals come from intermediate gas-phase HCN or if they are formed during the catalytic decomposition of $CH_3CN$.

Here we utilize either $CH_3CN^{15}$ or $CH_3C^{13}N$ to label the pathways of C and N in the proposed intermediate C≡N units. We see that the two inequivalent carbons in $CH_3CN$ are incorporated into the $sp^2$ network of the SWNT in equal proportion, while the $N_2$ is formed from the $N^{15}$. We deduce that the direct catalytic processing of entire $CH_3CN$ molecules at the catalyst surface is the initial step in the reaction pathway leading to $N_2$-filled SWNTs.

## 2 Materials & methods

Vertically aligned single-walled carbon nanotubes (VA-SWNTs) were grown by no-flow chemical vapor deposition.[10,15] We used either 1.5 vol% $CH_3CN^{15}$ added to ethanol feedstock or pure $CH_3C^{13}N$ to synthesize vertically aligned SWNTs containing $N_2^{15}$ or $N_2^{14}$. The $CH_3CN^{15}$ and $CH_3C^{13}N$ were purchased from Cambridge Isotope Laboratories, Inc. The isotope purity is given to be >98%. X-ray photoelectron spectra (XPS) were recorded with a PHI 5000 VersaProbe setup. X-ray absorption spectroscopy (XAS) was conducted at beamline BL27SU at the SPring-8 synchrotron facility. The beamline is dedicated to soft X-ray absorption spectroscopy.[16,17] To maximize the signal intensity from the encapsulated $N_2$ molecules (~600 ppm) we used a slit-limited resolution of 80 meV, a stepsize of 10 meV and an acquisition time of 3 s. Additionally, all spectra were recorded at 75° grazing incidence using *p*-polarized X-rays for maximum attainable peak intensities.[13] We normalized the XAS spectra by dividing the drain current of the samples by the simultaneously

[a]*University of Vienna, Vienna, Austria. E-mail: c.kramberger-kaplan@univie.ac.at; Fax: +43 14277 51375; Tel: +43 14277 72628*
[b]*University of Tokyo, Tokyo, Japan*
[c]*SPring-8, Sayo, Japan*
† Present address: Maejo University, Chiang Mai, Thailand.
‡ Present address: University at Buffalo, Buffalo, USA.

recorded drain current at the last focusing mirror. To obtain the best possible comparison, $N_2^{15}$ and $N_2^{14}$@VASWNTs were always mounted onto the same sample holder and were always measured without any delay using identical settings.

# 3 Results & discussion

## 3.1 Stoichiometry of N and C

The high yield of $N_2$ over pyridinic or substitutional N bonding was confirmed by XPS. Fig. 1 shows the survey scan of clean, as-synthesized $N_2^{15}$@VA-SWNTs in the lower panel. During the root growth process the CoMo catalyst particles stay attached to the substrate and only pure SWNTs emerge upwards. Hence, the single prominent spectral feature is the C1s at 284.6 eV. At this scale the O1s at 530 eV and N1s at 404 eV are hardly discernible. Detailed scans of the N1s and C1s region are shown above the survey scan. The C1s shows an asymmetric Doniach Šunjić lineshape with the secondary π electron shake up. The lineshape is typical for metallicity-mixed SWNTs.[18,19] The N1s shows a single prominent peak of molecular $N_2$ at 404.5 eV. The N1s and C1s were measured with identical resolution settings and can be directly compared. The atomic cross-section of nitrogen is 1.8 times that of carbon,[20] therefore the abundance of N as compared to C is ~600 ppm. If we assume a typical macroscopic density of VA-SWNT material to be 50 μg $cm^{-3}$, the density of stored $N_2$ would be equivalent to that of $N_2$ gas at 340 mbar and 0 °C. Inside densely packed SWNT bundles (1.3 g $cm^{-3}$) the stored density of $N_2$ would correspond to that of $N_2$ gas at 8.8 bar and 0 °C. The N/C stoichiometry of 600 ppm is approximately 10 times lower than the 1.5 vol% of $CH_3CN$ in $C_2H_5OH$ used during SWNT synthesis. The noisy signal just above 401 eV may be tentatively assigned to traces of $NO_x$. The signal from substitutional or pyridinic N is expected to be in the range from 398–400 eV, and is evidently not detectable.

## 3.2 Fractionation of $C^{13}$ and $C^{12}$

Isotope labeling of the carbons in the feedstock is a viable technique for investigating reaction pathways. We grew SWNTs from pure $CH_3C^{13}N$ and regular $CH_3CN$. The Raman spectra of these two samples are shown in Fig. 2.

The high-frequency optical phonon modes undergo a softening and broadening due to the increased mass and phonon–phonon scattering rates.[22–24] The G mode of SWNTs synthesized from pure isotopic $CH_3C^{13}N$ reveals a significant downshift. The actual concentration of $C^{13}$ can be readily calculated from eqn (1)

$$\omega(c) = \omega_N \sqrt{\frac{12 + 0.011}{12 + c}} \quad (1)$$

here $\omega_N$ is the G-band frequency of naturally occurring $C^{12}$ material, which contains 1.1% $C^{13}$. The observed maxima of the tangential G modes $\omega_N = 1594.8$ and $\omega(c) = 1564.3$ yield an abundance $c = 48\%$ $C^{23}$ in the nanotube walls. The $C^{12}$ and $C^{13}$ in $CH_3C^{13}N$ have—under the current conditions—roughly the same probability to contribute to growth. The reaction pathways in ethanol have only been recently elucidated in a study using site-selectively isotope-labeled $C_2H_5OH$, where either one or both of the C atoms were replaced with $C^{13}$. In particular it was demonstrated that under equivalent synthesis conditions the reaction pathway for ethanol is dominated by catalytic decomposition, which has a balanced isotope fractionation.[25]

The even fractionation of both inequivalent C atoms strongly suggests that the entire $CH_3CN$ molecule arrives at the catalytic site, where it is then further processed. We conclude that at 800 °C thermal decomposition is negligible since the initial dehydrogenation step is thermally inaccessible.[21] Detailed reaction processes on the catalyst particle during the synthesis are, however, obscured from macroscopic post-synthesis investigations.

In our specific case a scenario may be devised by considering the binding energies. The binding energy of C≡N is 891 kJ $mol^{-1}$ and that of free $C_2$ is calculated to be on the order of 300 kJ $mol^{-1}$.[21,26] We suggest that during dissolution the C–C bond and all H bonds in $CH_3CN$ break, after which both C and C≡N diffuse into or on the metal catalyst particle. The inert $N_2$ is released when two C≡N react. The individual steps are

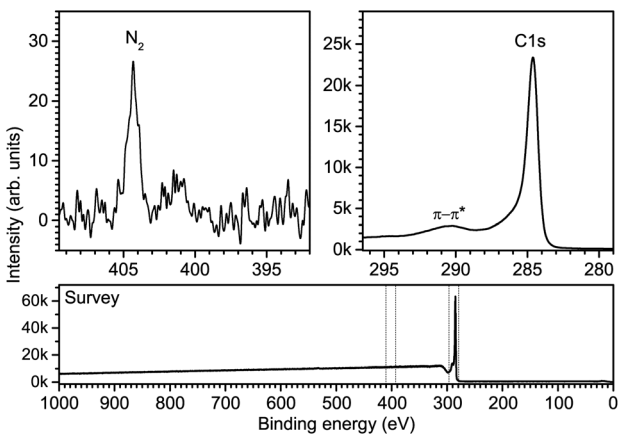


Fig. 1 XPS spectra of N1s (top left), C1s (top right) and survey scan (bottom) of $N_2^{15}$@VA-SWNTs.

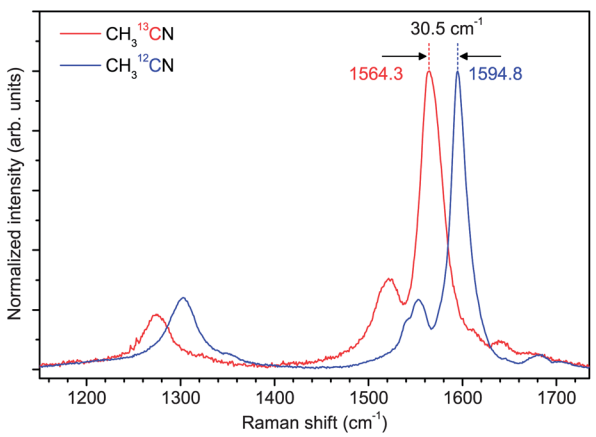


Fig. 2 Raman spectra of SWNTs made of natural $C^{13}$ : $C^{12}$ = 99 : 1 (blue) and $C^{13}$ : $C^{12}$ = 48 : 52 (red). The excitation wavelength is 633 nm.

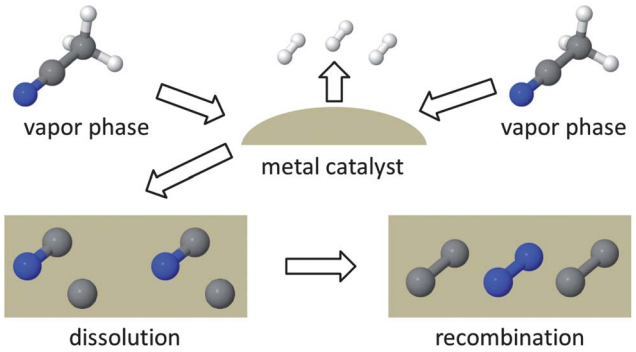


Fig. 3 Steps in the proposed reaction pathway from $CH_3CN$ to dissolved $C_2$ and inert $N_2$.

illustrated in Fig. 3. This pathway implies that all the N from $CH_3CN$ is processed *via* the catalyst particle before it is released as inert $N_2$.

In the case of pure $CH_3CN$ feedstock there is clearly not enough room inside the SWNT to accommodate all the $N_2$ that is expelled from the active catalyst particle. Even at sufficiently low concentrations of N (*e.g.*, less than 3 vol% would roughly correspond to the saturation value of 1 at%), most of the $N_2$ is released into the environment. The low trapping probability is in accordance with reduced nanotube diameters rooting from larger sized catalyst particles.[10] In the perpendicular growth mode, most of the catalyst particle surface area is not covered by the growing nanotube.[27] Therefore the size of the catalyst particle determines the trapping efficiency of $N_2$, but it does not determine the diameter of the growing nanotubes.

### 3.3 Isotope shift in $N_2^{15}$

X-ray absorption is the method of choice to investigate the possible isotope shift in the vibron energy of $N_2$. With the natural isotope abundance of over 99% $N^{14}$, the equidistant satellites in the XAS spectrum are separated by 233 ± 2 meV.[28] For pure $N^{15}$ a spacing of 225 ± 2 meV is expected from scaling with $\sqrt{1/m}$. The isotope shift in the vibrons of isotope mixed $N^{14}N^{15}$ was observed by Raman spectroscopy to be 4 meV.[29] At a full width at half maximum of 140 meV and a typical uncertainty of ±2 meV, very smooth spectra from a ~600 ppm fraction in the specimen are required to reveal the subtle isotope shift. The XAS spectra in Fig. 4 show the normalized data before and after background subtraction. The lowest resonance energy corresponds to the direct N1s absorption event, and higher resonance energies correspond to the concomitant excitation of one or more vibrons. The isotope shift between $N_2^{14}$ and $N_2^{15}$ may already be visible to the trained eye in the original spectra. After subtracting the background, it is much easier to recognize the equidistant series of four well-resolved peaks. A fifth peak is included in the fitting procedure, but its relative weight is considered insufficient for quantitative comparison.

The four Voigtian peaks that are resolved with reliable peak positions reveal an increasing offset due to the isotope shift. The peak positions are marked by vertical lines, and seem to be systematically shifted to lower resonance energies with

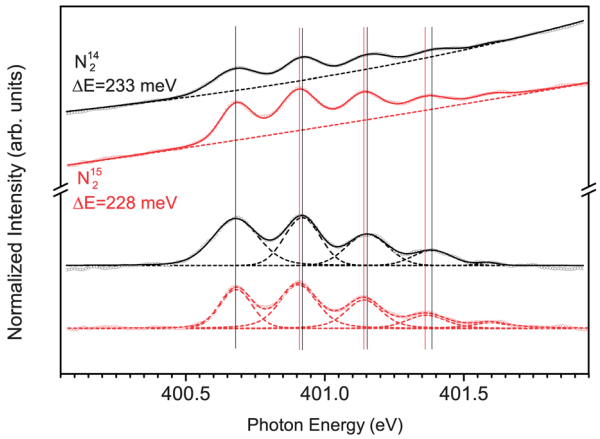


Fig. 4 High resolution XAS of the vibron satellites in the N1s resonance of $N_2^{14}$ (black) and $N_2^{15}$ (red)@VA-SWNTs. Raw data are circles, solid lines are fits and dashed lines are individual peaks or the background, respectively.

increasing vibron numbers. We find an average vibron energy of 228 ± 2 meV, which is in reasonable agreement with the expected value. We are surely at the limit of how accurately the peak positions could be determined from the actual line shapes in one individual spectrum, yet the direct comparison of the N1s region of $N_2^{14}$ and $N_2^{15}$ shows a noticeable isotope shift. The biggest isotope shift is expected for the fourth peak, and would be 24 meV (or halfway between 2 and 3 data points). This corresponds to the shift in peak position that is visible in the actual data and is within experimental accuracy.

The obtained N1s XAS spectra confirm the expected isotope shift of $N_2^{14}$ and $N_2^{15}$. Moreover, following the synthesis and XPS measurement the samples were stored for over six months under ambient conditions until the scheduled beamtime at SPring-8. The extended period over which $N_2^{15}$ was retained proves that the as-grown capped SWNTs are tight molecular containers.

## 4 Conclusions

We used isotope-labeled acetonitrile $CH_3C^{13}N$ and $CH_3CN^{15}$ to trace the reaction pathway from acetonitrile to SWNTs containing encapsulated $N_2$. The balanced incorporation of both inequivalent C atoms into acetonitrile, as evidenced by Raman spectroscopy, is the signature of a catalytic dissolution of the entire molecule. The very strong C≡N bond further suggests that all N molecules are present during dissolution in the catalyst metal. The geometry of a perpendicular growth mode limits the area for encapsulating $N_2$ that is released when two C≡N react at the catalyst particle. The vibron shift in the N1s X-ray absorption spectra clearly identifies stably encapsulated $N_2^{15}$ from $CH_3CN^{15}$ inside SWNTs.

## Acknowledgements

Beamtime at SPring-8 was granted for proposal 2013A1107. CK is an APART fellow (Grant no. A-11456) of the Austrian Academy

of Sciences. TT is supported by the office of the higher education commission of Thailand.

## References

1 M. Terrones, R. Kamalakaran, T. Seeger and M. Ruhle, *Chem. Commun.*, 2000, 2335–2336.
2 H. C. Choi, S. Y. Bae, W.-S. Jang, J. Park, H. J. Song, H.-J. Shin, H. Jung and J.-P. Ahn, *J. Phys. Chem. B*, 2005, **109**, 1683–1688.
3 J. Liu, Y. Zhang, M. I. Ionescu, R. Li and X. Sun, *Appl. Surf. Sci.*, 2011, **257**, 7837–7844.
4 J. G. Zhou, J. A. Wang, H. Liu, M. N. Banis, X. L. Sun and T. K. Sham, *J. Phys. Chem. Lett.*, 2010, **1**, 1709–1713.
5 A. V. Okotrub, L. G. Bulusheva, A. G. Kudashov, V. V. Belavin, D. V. Vyalikh and S. L. Molodtsov, *Appl. Phys. A: Mater. Sci. Process.*, 2009, **94**, 437–443.
6 A. V. Okotrub, M. A. Kanygin, L. G. Bulusheva and D. V. Vyalikh, *Fullerenes, Nanotubes, Carbon Nanostruct.*, 2010, **18**, 551–557.
7 P. Ayala, A. Grüneis, C. Kramberger, M. H. Rümmeli, I. G. Solorzano, F. L. Freire Jr and T. Pichler, *J. Chem. Phys.*, 2007, **127**, 184709.
8 E. M. M. Ibrahim, V. O. Khavrus, A. Leonhardt, S. Hampel, S. Oswald, M. H. Rummeli and B. Buchner, *Diamond Relat. Mater.*, 2010, **19**, 1199–1206.
9 P. Ayala, R. Arenal, A. Loiseau, A. Rubio and T. Pichler, *Rev. Mod. Phys.*, 2010, **82**, 1843–1885.
10 T. Thurakitseree, C. Kramberger, P. Zhao, S. Aikawa, S. Harish, S. Chiashi, E. Einarsson and S. Maruyama, *Carbon*, 2012, **50**, 2635–2640.
11 T. Thurakitseree, C. Kramberger, A. Kumamoto, S. Chiashi, E. Einarsson and S. Maruyama, *ACS Nano*, 2013, **7**, 2205–2211.
12 R. E. Barajas-Barraza, J. A. Ramirez-Ruiz and R. A. Guirado-Lopez, *J. Comput. Theor. Nanosci.*, 2008, **5**, 2255–2263.
13 C. Kramberger, T. Thurakitseree, H. Koh, Y. Izumi, T. Kinoshita, T. Muro, E. Einarsson and S. Maruyama, *Carbon*, 2013, **55**, 196–201.
14 J. H. Yang, D. H. Lee, M. H. Yum, Y. S. Shin, E. J. Kim, C. Y. Park, M. H. Kwon, C. W. Yang, J. B. Yoo, H. J. Song, H. J. Shin, Y. W. Jin and J. M. Kim, *Carbon*, 2006, **44**, 2219–2223.
15 H. Oshima, Y. Suzuki, T. Shimazu and S. Maruyama, *Jpn. J. Appl. Phys.*, 2008, **47**, 1982–1984.
16 H. Ohashi, E. Ishiguro, Y. Tamenori, H. Okumura, A. Hiraya, H. Yoshida, Y. Senba, K. Okada, N. Saito, I. H. Suzuki, K. Ueda, T. Ibuki, S. Nagaoka, I. Koyano and T. Ishikawa, *Nucl. Instrum. Methods Phys. Res., Sect. A*, 2001, **467**, 533–536.
17 H. Ohashi, E. Ishiguro, Y. Tamenori, H. Kishimoto, M. Tanaka, A. Irie, T. Tanaka and T. Ishikawa, *Nucl. Instrum. Methods Phys. Res., Sect. A*, 2001, **467**, 529–532.
18 C. Kramberger, H. Rauf, H. Shiozawa, M. Knupfer, B. Büchner, T. Pichler, D. Batchelor and H. Kataura, *Phys. Rev. B: Condens. Matter Mater. Phys.*, 2007, **75**, 235437.
19 P. Ayala, Y. Miyata, K. De Blauwe, H. Shiozawa, Y. Feng, K. Yanagi, C. Kramberger, S. R. P. Silva, R. Follath, H. Kataura and T. Pichler, *Phys. Rev. B: Condens. Matter Mater. Phys.*, 2009, **80**, 205427.
20 J. Scofield, *J. Electron Spectrosc. Relat. Phenom.*, 1976, **8**, 129–137.
21 A. Lifshitz and C. Tamburu, *Int. J. Chem. Kinet.*, 1998, **30**, 341–347.
22 F. Simon, C. Kramberger, R. Pfeiffer, H. Kuzmany, V. Zólyomi, J. Kürti, P. M. Singer and H. Alloul, *Phys. Rev. Lett.*, 2005, **95**, 017401.
23 C. Kramberger, M. Löffler, M. Rümmeli, A. Grüneis, R. Schönfelder, O. Jost, T. Gemming, T. Pichler and B. Büchner, *Phys. Status Solidi B*, 2006, **243**, 3050–3053.
24 S. D. Costa, C. Fantini, A. Righi, A. Bachmatiuk, M. H. Rümmeli, R. Saito and M. A. Pimenta, *Carbon*, 2011, **49**, 4719–4723.
25 R. Xiang, B. Hou, E. Einarsson, P. Zhao, S. Harish, K. Morimoto, Y. Miyauchi, S. Chiashi, Z. Tang and S. Maruyama, *ACS Nano*, 2013, **7**, 3095–3103.
26 S. Shaik, D. Danovich, W. Wu, P. Su, H. S. Rzepa and P. C. Hiberty, *Nat. Chem.*, 2012, **4**, 195–200.
27 M. F. C. Fiawoo, A. M. Bonnot, H. Amara, C. Bichara, J. Thibault-Penisson and A. Loiseau, *Phys. Rev. Lett.*, 2012, **108**, 195503.
28 C. T. Chen, Y. Ma and F. Sette, *Phys. Rev. A: At., Mol., Opt. Phys.*, 1989, **40**, 6737–6740.
29 M. Musso, F. Matthai, D. Keutel and K. L. Oehme, *J. Chem. Phys.*, 2002, **116**, 8015–8027.

 